ACS APPLIED MATERIALS & INTERFACES

Research Article

www.acsami.org

Bioinspired Porous Octacalcium Phosphate/Silk Fibroin Composite Coating Materials Prepared by Electrochemical Deposition

Ya Yang,[†] Hui Wang,*[,†,‡] Feng-Yi Yan,[†] Yu Qi,[†] Yue-Kun Lai,[†] Dong-Mei Zeng,[†] Guoqiang Chen,[†] and Ke-Qin Zhang*[,†,‡]

[†]National Engineering Laboratory for Modern Silk, College of Textile and Clothing Engineering, Soochow University, Suzhou 215123, P. R. China

[‡]Research Center of Cooperative Innovation for Functional Organic/Polymer Material Micro/Nanofabrication, Soochow University, Suzhou 215123, P. R. China

ABSTRACT: The biomimetic structure and composition of biomaterials are recognized as critical factors that determine their biological performance. A bioinspired nano-micro structured octacalcium phosphate (OCP)/silk fibroin (SF) composite coating on titanium was achieved through a mild electrochemically induced deposition method. Findings indicate that SF plays a critical role in constructing the unique biomimetic hierarchical structure of OCP/SF composite coating layers. In vitro cell culture tests demonstrate that the presence of OCP/SF composite coatings, with highly ordered and hierarchically porous structure, greatly enhance cellular responses. The coatings developed in this study have considerable potential for various hard tissue engineering and applications.

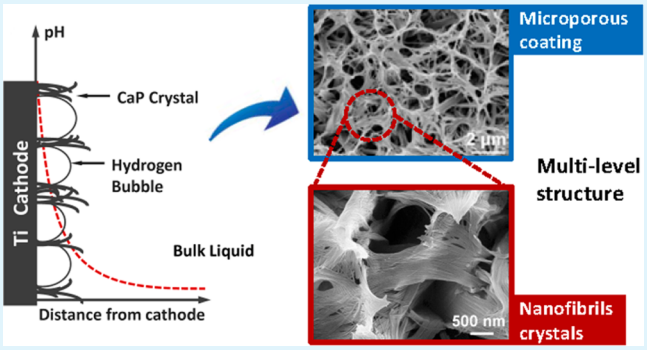

KEYWORDS: *silk fibroin, OCP, composite coating, nano-micro structure, cell culture*

1. INTRODUCTION

Many living organisms found in nature exhibit fascinating multiple functionalities, which arise from the multilevel surface structures and chemical compositions found in their biology.[1−4] Natural bone displays such multifunctionality, with properties including strong mechanical strength, ability to accommodate abundant blood vessels and marrow, as well as nutrients and oxygen transport. These bone functions originate from its hierarchical structure and multiple chemical compositions, which mainly consist of calcium phosphate (CaP) and organic protein matrix.[5,6] Inspired by the multifunctionality displayed by natural bone, the purpose of this study was to design and fabricate biomimetic multiscale structured composite materials for achieving multifunctional integration in tissue engineering. The goal of our findings was to provide an implant coating material for accelerated bone regeneration, especially for load-bearing osteoregenerative applications.

Since the scientific world gained understanding on the composition of natural bone, calcium phosphates and biological polymers hybrid coating materials on biomedical metals have been a source of extensive interest because of their biomedical merits. Recently, researchers became interested in developing CaP/collagen composite coating on the surface of titanium substrate, in order to accelerate bone growth and implant fixation in vivo.[7−9] However, collagen originating from cattle may have problems, including transmission of disease and high price.[10] *Bombyx mori* (silkworm) silk has recently gained increasing attention as a biomaterial because of its biocompatibility, relatively slow degradation in vivo, ease of processing into various formats, excellent mechanical performance, and sufficient supply and ease of acquiring from the mature sericulture industry.[11−20] It is superior to commonly used biological polymers such as collagen and poly(L-lactic acid) (PLA).[21−23] Octacalcium phosphate ($Ca_8H_2(PO_4)_6{\cdot}5H_2O$, OCP) is a significant calcium phosphate regarded as a precursor of biological apatite and eventually converts into hydroxyapatite.[24−27] Since increasing osteoblast adhesion on nanomaterials was reported in 1999,[28] further research has shown that the unique properties of nanomaterials can lead to development of novel tissue substitution and improving performances in both biology and mechanics.[29−31] In recent years, researchers have focused on the critical effect of microstructures on the biological performance of biomaterials. Furthermore, designing and fabricating composite biomaterials with a biomimetic multiscale structure have been a challenge for the researchers in the area of materials and biology.

In this study, a highly ordered nano-micro multiscale OCP/SF composite coating on a titanium (Ti) substrate was constructed by electrochemical deposition technique (ED). ED was used in this experiment because it can be performed in

Received: April 9, 2014
Accepted: March 3, 2015
Published: March 3, 2015

DOI: 10.1021/am5088488
ACS Appl. Mater. Interfaces 2015, 7, 5634−5642

mild conditions, as well as more controllable deposition conditions.[32−34] ED technique can induce the coprecipitation of SF and OCP minerals at the cathode to form a uniform, crack-free, and bone-like composite coating, as long as deposition parameters are well controlled. Under effect of electric field, SF plays an important role in controlling the OCP crystal growth behavior, forming a homogeneous mixture with calcium phosphate minerals, resulting in a unique nano-micro multiscale biomimetic structure. In vitro cell culture was performed to demonstrate material biocompatibility, and explore the biomedical applications of the nano-micro structured OCP/SF composite coating.

2. MATERIALS AND METHODS

2.1. Pretreatment of the Ti Substrates. Working electrodes (cathodes) were made from 10 mm × 10 mm × 2 mm commercial pure Ti plates. Ti plates were polished with silicon carbide paper ranging from grit 200−1000 (200 grit/interval) and then sculptured in an acidic mixture solution containing 10% (*v*/*v*) HNO_3 and 1% (*v*/*v*) HF to remove impurities. Finally, Ti plates were ultrasonically cleaned with acetone, ethyl alcohol, and deionized water, consecutively for 15 min each, and then stored in deionized water.

2.2. Preparation of Composite Coatings. Silkworm cocoons were boiled for 40 min in an aqueous solution of 0.5% (*w*/*v*) Na_2CO_3 and then rinsed thoroughly with distilled water to remove silk sericin. The purified SF fibers were dissolved in 9.3 mol/L LiBr solution at 60 °C for 1 h. The solution was dialyzed in deionized water using a cellulose dialysis membrane (MWCO 6000−8000 Da, Spectra/Por, U.S.A.) at room temperature for 3 days to remove LiBr. The dialyzed SF aqueous solution was collected and stored at 4 °C until further use.

Electrochemical deposition (ED) was carried out in a three-electrode electrochemical cell controlled by an electrochemical workstation (CHI600D, Shang Hai Chen Hua Instrument Company, China). A Ti plate was used as the working electrode (cathode); the counter and reference electrodes were platinum sheet and saturated calomel electrode, respectively. The effects of some ED process parameters, i.e., concentration, temperature, current density, and duration, were systematically investigated. In this study, the OCP and OCP/SF coatings prepared under the optimum deposition parameters. The initial electrolyte solution contained 0.045 mol/L $Ca(NO_3)_2 \cdot 4H_2O$ and 0.027 mol/L $NH_4H_2PO_4$; SF was added to the electrolyte at a concentration of 1.0 mg/mL, and its pH was adjusted to 4.2. The calcium phosphate and silk fibroin (CaP/SF) composite coatings were prepared at a constant cathodic current density of 0.5 mA/cm^2 for 15 min. During the ED process, the electrochemical cell with electrolyte was immersed in a water bath to maintain the temperature close to 75 °C. For comparison, the pure calcium phosphate (CaP) coating obtained in the electrolyte without SF was used as control, keeping all other deposition parameters the same. After the ED process, the final samples were rinsed with abundant deionized water and dried in the air. SF powder was gathered from freeze-dried SF aqueous solution. The OCP powder used for the mechanical mixture was synthesized by a hydrothermal method. $Ca(NO_3)_2 \cdot 4H_2O$ and $NH_4H_2PO_4$ were added to distilled water to obtain a Ca/P mole ratio of 1.40. The resultant suspension was controlled pH of 4.0 and stirred. Then the samples were placed in a Teflon-lined stainless steel vessel and hydrothermally treated at 100 °C for 2 h. The precipitate was washed by distilled water, collected by filtration and dried at 50 °C in a dry oven. The mechanical mixture of SF powder and pure synthetic CaP powder (CaP/SF) were pressed into pellets as controls.

2.3. Characterization of Prepared Coatings. Scanning electron microscopy (SEM; S4800, Japan) was used to observe the morphology of the prepared coatings. Before the observation, the samples were sputtered with platinum. The crystal size distribution of prepared coatings was analyzed from SEM images using image J software (ImageJ1.44p, National Institutes of Health, U.S.A.). The crystalline structure of the samples was examined using X-ray diffraction (XRD, PANalytical X'pert-PRO, Netherland) with Cu Kα radiation source at 40 kV and 30 mA in a 2θ range from 4° to 60°. Fourier transform infrared spectroscopy (FTIR, Nicolet-5700, U.S.A.) was employed in transmission mode using the KBr technique to analyze the chemical composition of the coatings. Thermogravimetric analysis was run under the flow of nitrogen gas at a scanning speed of 15 °C min^{-1} (between 38 and 800 °C) by using a rheometric scientific TGA 1000 (U.S.A.). The chemical state of the coatings was determined using X-ray photoelectron spectroscopy (XPS, Axis Ultra HASAl-Kα source, U.K.). The charging shift was compensated for the main C 1s component by setting a value of 284.6 eV. The water contact angles were measured at ambient temperature using an OCA-40 contact angle instrument (Dataphysics, Germany) with a drop volume of 6 μL. Deionized water (Millipore, 18 MΩ·cm) was employed as the source for contact angles measurement. All reported contact angle values were averaged from the four drops at different locations of the samples surface.

2.4. Biological Evaluation Based on in Vitro Cell Culture. Preosteoblast cells MC3T3-E1 were expanded in alpha minimum essential medium (α-MEM, Thermo Fisher Scientific, U.S.A.) containing 10% fetal bovine serum (FBS, Life Technologies, U.S.A.) and 1% penicillin/streptomycin (Life Technologies, U.S.A.). Human umbilical cord-derived mesenchymal stem cells (HUMSCs) were cultured in low-glucose Dulbecco's modified Eagle's medium (DMEM, Thermo Fisher Scientific, U.S.A.) with 10% fetal bovine serum (FBS, Invitrogen, U.S.A.) and 1% penicillin/streptomycin (Invitrogen, CA). All cells were incubated at 37 °C in a humidified atmosphere with 5% CO_2, and the medium was replaced every 48 h. After culturing in growth medium until 80%−90% confluence, the cells were harvested to seed onto the coated samples.

Sterilized samples (10 mm × 10 mm × 2 mm) were transferred into 24-well plastic culture plates. MC3T3-E1 cells and HUMSCs were seeded onto the prepared OCP/SF coatings, with pure OCP coatings and a mechanical mixture of pure CaP and SF used as control, at a density of 1 × 10^5 cells per sample. Cells were incubated in culture medium (1 mL/well) at 37 °C under 5% CO_2 atmosphere for 1, 3, and 7 days, with the medium replaced every 3 days until harvested.

Cell viability and proliferation were measured by 3-(4,5-dimethylthiazol-2-yl)-2,5-diphenyl tetrazolium bromide (MTT; Sigma, U.S.A.) staining. At desired time points, the cell-seeded samples were incubated in MTT solution (5 mg/mL MTT in cell culture medium) in a 5% CO_2 incubator at 37 °C for 4 h. The intense purple formazan derivative formed via cell metabolism was eluted and dissolved in dimethyl sulfoxide (DMSO) with a dosage of 400 μL/well. The absorbance was measured at 570 nm with a reference wavelength of 690 nm using a microplate reader (BioTek Synergy4, U.S.A.). Cell number was correlated to optical density (OD).

To determine the morphology of cell growth, cell-seeded samples were examined under scanning electron microscopy (SEM, S4800, Japan) at desired time points. Cell-seeded samples were gently washed three times with cold 0.1 M phosphate buffer, fixed by 2.5% glutaraldehyde for 2 h at 48 °C, washed with 0.1 M phosphate buffer (4 °C) three times at 15 min intervals each, and then dehydrated through a series of graded alcohols. The samples were dried in a critical point drier (HCP-2 HITACHI, Japan) and sputtered with a thin gold film for SEM observation.

Fluorescein diacetate (FDA) molecule probe was used as a viable cell marker[35] to investigate the growth of cells on the prepared coatings. At the designated time points (1, 3, and 7 days), the cell-seeded samples were washed with PBS, then incubated with 30 μg/mL FDA solution for 15 min, and washed with PBS. The positive cells were observed immediately under laser confocal microscope (Olympus FluoView 1000, Japan).

2.5. Statistical Analysis. All data were expressed as means ± standard deviations (SD). The statistical significance of differences among each group was examined by the *t* test. Significance was set at $p < 0.05$ level.

DOI: 10.1021/am5088488
ACS Appl. Mater. Interfaces 2015, 7, 5634−5642

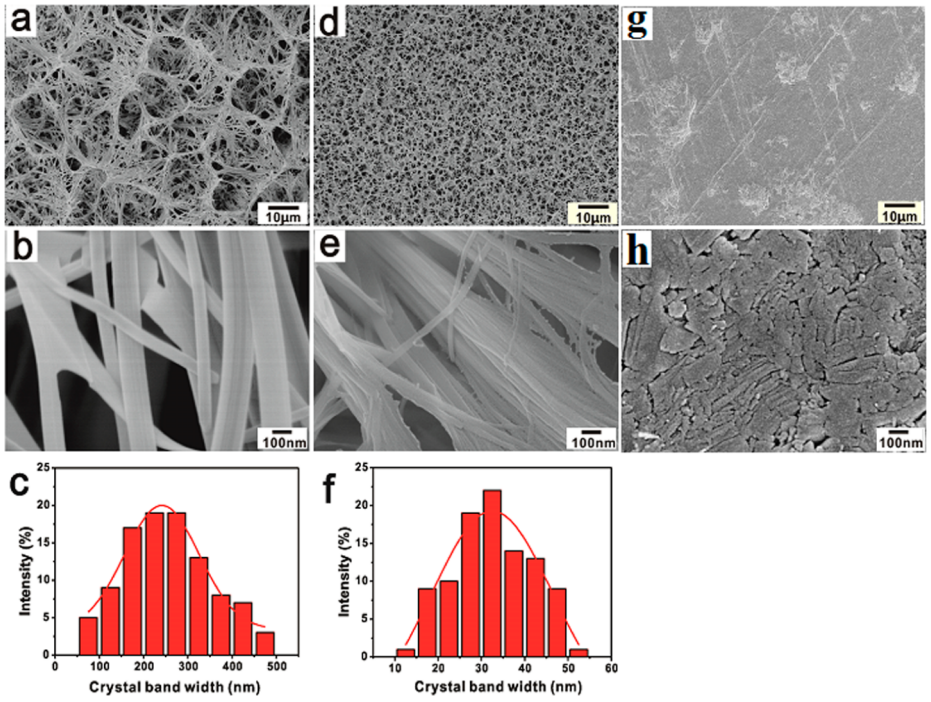

Figure 1. SEM images of the prepared coatings in the absence (a, b) and presence (d, e) of SF, and mechanical mixture of CaP/SF (g, h). The width distribution of the CaP fibrils in the absence (c) and presence (f) of SF.

3. RESULTS

3.1. Hierarchical Microstructure of the Composite Coatings. The morphology of prepared coatings with and without SF, together with the width distribution of the OCP fibrils on the prepared coatings, and the morphology of mechanical mixture samples of CaP/SF, are shown in Figure 1. In the ED process without SF, the pure CaP coating control formed on the surface of Ti substrate exhibits an ordered porous structure with average pore diameter of 10−15 μm

High magnification SEM image (Figure 1b) and width distribution of the OCP crystals (Figure 1c) show that the ordered porous coating was comprised of ribbon-like crystals with the width of 250 ± 98 nm. In the presence of SF, the ordered porous coating is still retained on the Ti substrate after the ED process (Figure 1d). Nevertheless, the width and pore dimensions of OCP/SF coating are reduced distinctly (Figure 1d−f). The coating exhibited a uniform higher ordered nano-micro multiscale structure: microstructures with a porous topography in several micrometers (3−9 μm) and nanostructures of fibrils with an average width of 35 ± 10 nm. This indicates that SF can affect the growth behavior of CaP minerals, inhibiting and reducing the width of CaP crystals into the nanoscale. The morphology of CaP/SF mechanical mixture exhibited a flat surface without porous structure (Figure 1g). From the high magnification SEM image (Figure 1h), the flat surface was composed of numerous stacked nanoparticles. Other studies have shown that the hierarchical nano/micro materials interface can lead to novel tissue substitute and improve performance of both biology and mechanics.[29−31] This implies that the OCP/SF composite coating, with their highly ordered multiscale structure and larger surface area, may display excellent biological performances.

3.2. Crystalline Structure of the Samples by XRD. The crystalline structures of the prepared coatings with and without SF, and a mechanical mixture of CaP/SF were identified by XRD, as shown in Figure 2. The spectra of pure SF powder exhibited a peak at 2θ = 24−25°, attributing to the silk I

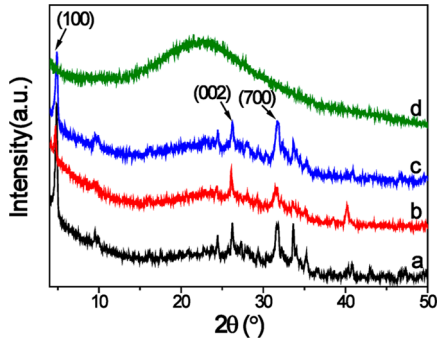

Figure 2. XRD spectra of the coating powder scraped off the Ti plates: (a) CaP coatings, (b) CaP/SF composite coating, (c) mechanical mixture of CaP/SF, and (d) pure SF powder.

crystalline structure.[36] The XRD curves indicate that, in all prepared samples, the main crystalline phases of CaP formed on the Ti surface was octacalcium phosphate ($Ca_8H_2(PO_4)_6 \cdot 5H_2O$, OCP; refer to JCPDS no. 44-778). The spectra of the powders scraped from the coatings exhibited a typical diffraction peak at 2θ = 4.7°, corresponding to the (100) plane of OCP. Compared to the pure CaP coating and mechanical mixture of CaP/SF, the spectrum of the OCP/SF coating powder (curve b) displayed a significant reduction in the relative intensities of the (100) and (700) reflections (Figure 2a). This implies that the SF most likely adsorbed on the (100) face of OCP to suppress the growth in this direction.[7]

3.3. Chemical Composition of the Samples. *3.3.1. Fourier Transform Infrared Spectroscopy.* FTIR spectroscopy was used to examine the chemical structure for the prepared

DOI: 10.1021/am5088488
ACS Appl. Mater. Interfaces 2015, 7, 5634−5642

coatings, as shown in Figure 3. It was observed that the characteristic FTIR absorption peaks of OCP, in particular that

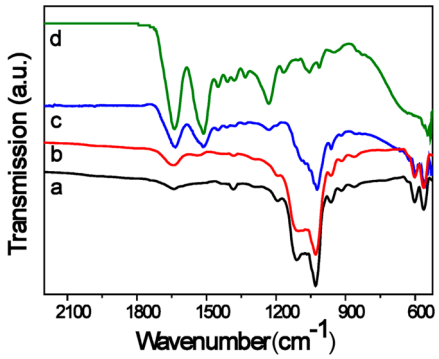

Figure 3. FTIR spectra of the (a) pure CaP coatings, (b) CaP/SF composite coating, (c) mechanical mixture of CaP/SF, and (d) pure SF powder.

of the P−O bands (at 1105 and 1029 cm^{-1}) and HPO_4^{2-} bonds (at 917 and 860 cm^{-1}), were observed in the prepared OCP coatings, OCP/SF composite coatings and CaP/SF mechanical mixture.[5,31] Two distinct peaks at 1640 (amide I, overlapped with OH absorption from H_2O molecules at 1636 cm^{-1}) and 1527 cm^{-1} (amide II) were assigned to SF; they appeared in prepared OCP/SF coating and mechanical mixture of CaP/SF. This indicates that SF is present on the OCP/SF composite coating and the mechanical mixture. FTIR results, together with SEM results, concluded that CaP/SF mechanical mixture samples have a composition that is similar to OCP/SF composite coatings but different surface structures. Furthermore, the β-sheet secondary structure fraction of SF in OCP/SF coating is low, while random coil dominates. The results imply that the electric field created in this ED process does not obviously change the dominant secondary structure of SF when SF solution is incorporated into the OCP/SF coating. The main role of the electric field is to drive the SF molecules to move toward and interacting with CaP crystals, influence OCP crystal growth behavior, and further modify the morphological structure of OCP/SF coating.

3.3.2. Thermogravimetric Analysis. Thermogravimetric curves of the prepared samples are shown in Figure 4. The initial weight loss of all the samples at about 100 °C is due to loss of moisture. The second weight loss took place in the temperature ranged from 250 to 400 °C. This is associated with the loss of SF. Based on the results of thermogravimetric

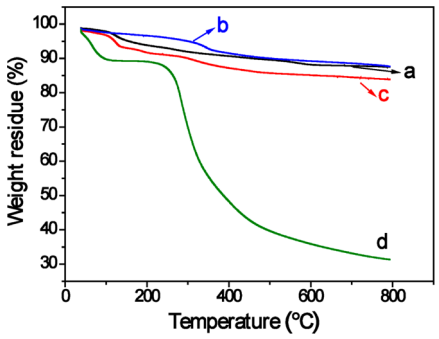

Figure 4. Thermogravimetric curves of the (a) pure CaP coatings, (b) CaP/SF composite coating, (c) mechanical mixture of CaP/SF, and (d) pure SF powder.

analysis, the concentration of SF in the OCP/SF composite coating is about 2.5 wt %. The mechanical mixture exhibits a similar composition of the coating with the concentration of SF being about 3.4 wt %.

3.3.3. X-ray Photoelectron Spectroscopy. In order to verify the chemical composition of the prepared coatings, XPS analysis was performed. The XPS results show that the elements present in the OCP/SF composite coating surface not only comprise C, Ca, P, and O but also contain N, as shown in Figure 5. Furthermore, the C peak intensity of curve b

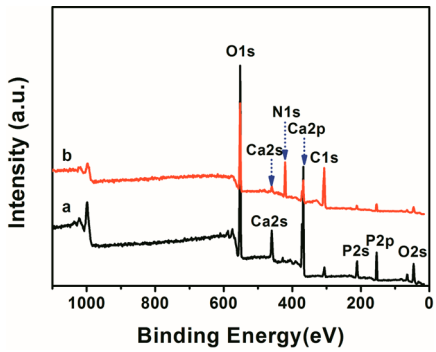

Figure 5. XPS survey spectra of the OCP coating (a) and OCP/SF composite coating (b).

increased in a visible manner. The above evidence reveals that the SF is actually present in the prepared OCP/SF composite coating after the ED process. The data collected here is consistent with the findings from FTIR analysis, allowing a conclusion regarding OCP/SF composite coating formation to be reached.

3.4. Wettability of the Prepared Samples. Images of water droplets lying on flat prepared sample surfaces and the corresponding contact angle values are shown in Figure 6. The

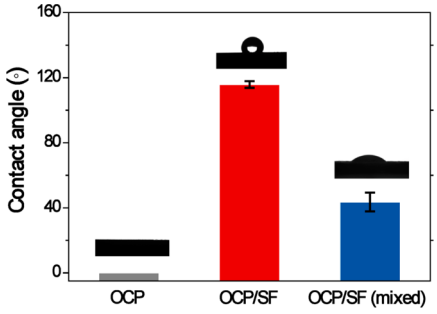

Figure 6. Water contact angles of the prepared pure OCP coatings, OCP/SF composite coatings, and mechanical mixture of CaP/SF. Data are mean ± SD.

water droplet quickly spreads and wetting of the pure OCP porous coating is observed, indicating such pure OCP porous coating is superhydrophilic. When SF was introduced, the water contact angles for the mechanical mixture of CaP/SF without porous structure increased to 43.6 ± 5.7°. On the OCP/SF composite coating, the water droplet forms a spherical shape with a higher water contact angle of about 115.8 ± 2.1°, showing that the hydrophobicity of the OCP/SF composite coating was enhanced. This was direct evidence of the multilevel nano-micro porous structure of the OCP/SF coating,

DOI: 10.1021/am5088488
ACS Appl. Mater. Interfaces 2015, 7, 5634−5642

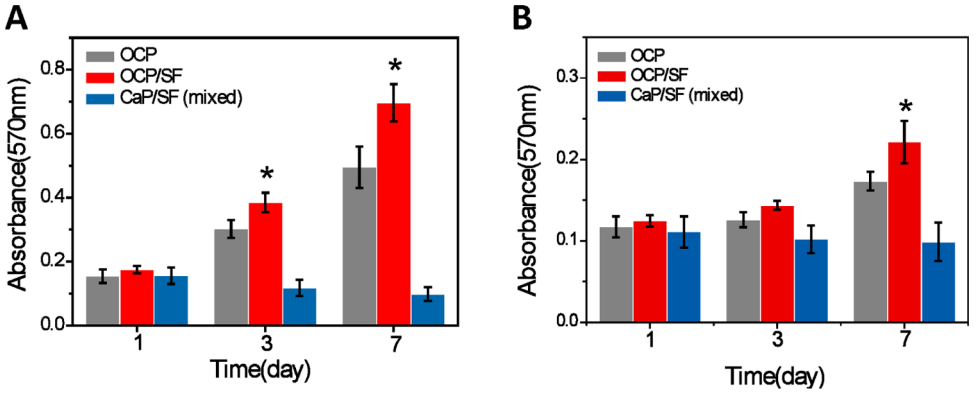

Figure 7. Preosteoblast MC3T3 cells (A) and HUMSCs (B) proliferation on the pure OCP coating, OCP/SF composite coating and mechanical mixture of CaP/SF for 1, 3, and 7 days. * denotes a significant difference between two groups at $p < 0.05$.

which mimicked that of the natural bone tissue, inducing a remarkable increase in its hydrophobicity.

3.5. Cell Proliferation and Morphology on the Prepared Coatings. *3.5.1. MTT Assay.* MTT assay was employed to compare the cell viability of the OCP/SF composite coatings to that of the OCP coatings and the mechanical mixture of CaP and SF (Figure 7). In order to investigate the cell response to the surface characteristics of prepared samples, preosteoblast MC3T3 cells and HUMSCs adhesion and proliferation were measured. There was a clear temporal proliferation profile of both cell types after 1, 3, and 7 days of culture on both OCP and OCP/SF coatings. However, it is worth to note that although the mechanical mixture of CaP/SF possessed the similar composition with OCP/SF coatings, it did not support greater cells proliferation for both MC3T3 cells and HUMSCs. It might be due to the very flat surface of the mechanical mixture of CaP/SF. It is evident that the smooth surface may retard cell attachment and proliferation.[37] In addition, the mechanical mixture of the CaP/SF sample was prepared by pressing SF powder (3.4 wt %) and synthetic CaP powder into pellets. Therefore, the proliferation failure may attribute to the limited surface contact between the cells and SF particles embedded in the mixed CaP/SF substrate and weak binding force between the SF and CaP powder. As shown in Figure 7, the preosteoblast MC3T3 cells' viability cultured on the OCP/SF coatings appeared significantly higher than that of the OCP coatings and mechanical mixture of CaP/SF at 3 and 7 day time points ($p < 0.05$); culminating in a viability 1.4 times higher than the OCP coatings and about 7.1 times higher than mechanical mixture of CaP/SF at 7 days. In the case of HUMSCs, live cells on the OCP and OCP/SF coatings surfaces were almost the same over the 3 days of the experiment (Figure 7B), while at 7 days, the cells cultured on the OCP/SF composite coating surface was significantly higher than on the other two control samples ($p < 0.05$). These results clearly indicate that the nano-micro multiscale porous structure within the OCP/SF coatings may promote the cells proliferate, allowing more cells to grow in a congenial environment.

3.5.2. Scanning Electron Microscopy. The SEM images exhibit the morphologies of inoculated MC3T3 cells and HUMSCs on the pure OCP coating, OCP/SF composite coating, and mechanical mixture of CaP/SF as shown in Figures 8 and 9, respectively. In comparison with the OCP coating, MC3T3 cells on the OCP/SF composite coating and mechanical mixture of CaP/SF after 1 and 3 days of cell culture showed a much higher degree of spreading (Figure 8), and cells

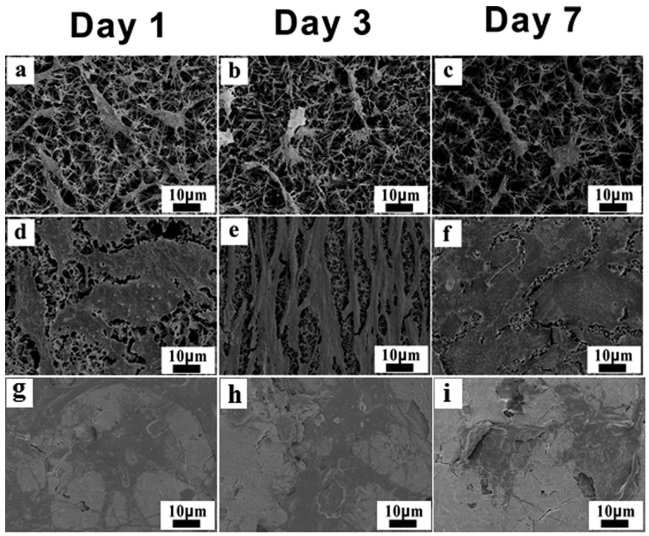

Figure 8. SEM micrographs of preosteoblast MC3T3 cells incubated on pure OCP coating (a–c), OCP/SF composite coating (d–f), and mechanical mixture of CaP/SF (g–i) for 1, 3, and 7 days, respectively.

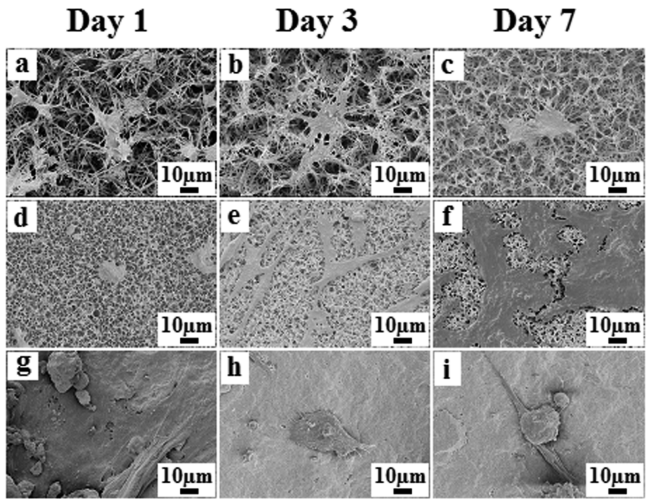

Figure 9. SEM micrographs of HUMSCs incubated on pure OCP coating (a–c), OCP/SF composite coating (d–f), and mechanical mixture of CaP/SF (g–i) for 1, 3, and 7 days, respectively.

on OCP and OCP/SF porous coating formed the cellular extension to bridge the adjacent micropores. After 7 days, the

DOI: 10.1021/am5088488
ACS Appl. Mater. Interfaces 2015, 7, 5634–5642

morphologies of MC3T3 cells grown on the OCP/SF composite coating showed a much thicker and denser attachment and formed the cell sheets, concealing the nano-micro porous structures of OCP/SF composite coating. In the case of HUMSCs, it is clearly seen that, after 1 day of culture, the cells exhibited uneven morphologies on the mechanical mixture of CaP/SF, and cells adhered and spread on the OCP/SF composite coating. After 3 days in culture, on the pure OCP/SF composite coating surface the cells showed spread and dense morphologies, while on the mechanical mixture of CaP/SF cells exhibited loose morphologies. After 7 days in culture, HUMSCs-seeded OCP/SF composite coating was covered by a cell sheet and with possible ECM formation. The inoculated both MC3T3 cells and HUMSCs attached and grew much better on the OCP/SF composite coating compared with pure OCP coating or mechanical mixture of CaP/SF.

3.5.3. Laser Confocal Microscopy. Laser confocal microscopy was carried out to study the dynamics of cell adhesion, spreading, and proliferation on prepared coatings after fluorescent straining with FDA as shown in Figures 10 and

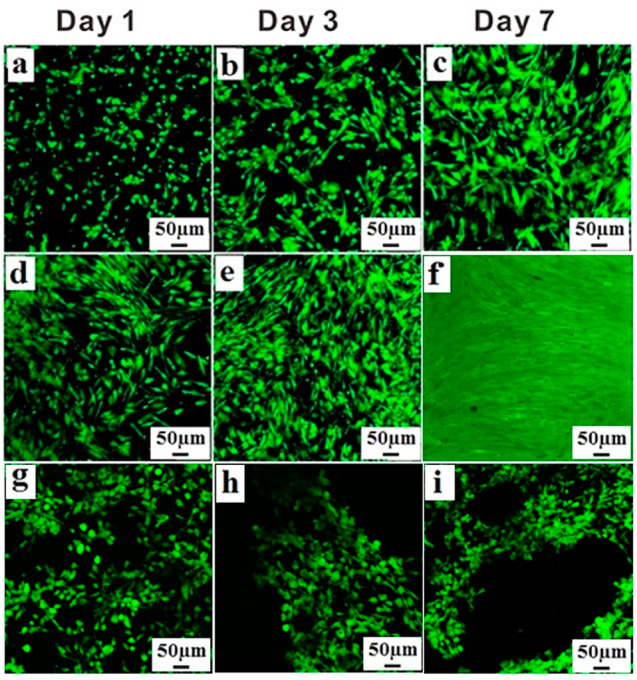

Figure 10. Laser confocal micrographs of preosteoblast MC3T3 cells incubated on pure OCP coating (a–c), OCP/SF composite coating (d–f), and mechanical mixture of CaP and SF (g–i) stained with FDA molecule probe for 1, 3, and 7 days, respectively.

11. MC3T3 cells were adhered to and spread on the OCP/SF composite coatings after 1 day in culture; these cells showed greater cells adherence and a higher degree of spreading than that of the pure OCP coatings and mechanical mixture of CaP/SF (Figure 10). Compared to the cells adhered on the OCP/SF coatings, fewer cells adhered to the mechanical mixture of CaP/SF. This poor adhesion was most likely due to its dense surface without porous structure, making nutrients difficult to run through the entire samples. After 3 days of cell culture, profuse cell growth was observed throughout the OCP/SF coatings compared to the OCP coating and mechanical mixture of CaP/SF, in which it was uncomparable. After 7 days, MC3T3 cells-seeded OCP/SF coatings were fully covered with a thick cell

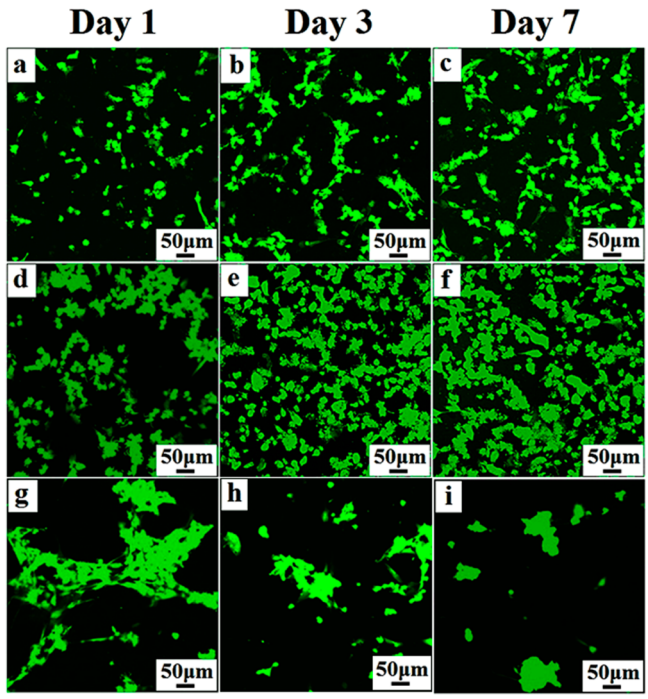

Figure 11. Laser confocal micrographs of HUMSCs incubated on pure OCP coating (a–c), OCP/SF composite coating (d–f), and mechanical mixture of CaP and SF (g–i) stained with FDA molecule probe for 1, 3, and 7 days, respectively.

multilayer. However, MC3T3 cells on mechanical mixture of CaP/SF showed a uneven morphology even after 7 days in culture. As shown in Figure 11, the spreading degree of HUMSCs on OCP/SF composite coatings was lower than that of MC3T3 cells. However, HUMSCs on OCP/SF composite coatings still showed greater cell attachment and better spreading during culture time.

4. DISCUSSION

All the experiments of cell culture has demonstrated that the electrochemically prepared OCP/SF composite coatings with ordered nano-micro porous structure on Ti substrate could improve cell adhesion, spreading, and proliferation of both MC3T3 cells and HUMSCs. The OCP coating shows the fluffier run-through porous structure on its surface. When cells contact the samples surface, cells need space for anchoring and also need sufficient space for spreading. However, the OCP crystals obtained in the OCP coating on titanium are preferentially orientation in the [002] direction or *c* axis. In other words, ribbon-like OCP crystals prefer to grow almost perpendicular to the titanium substrate. So the areas for cells anchoring and attachment are relatively small at the beginning period of cell culture. So cells on pure OCP coating show a few cell attachments but good spreading. Although OCP/SF composite coating and mechanical mixture of CaP/SF possessed similar composition, the OCP/SF composite coating with nano-micro multiscale porous structure shows excellent cell response. When SF is introduced, the surface area of the OCP/SF composite coating are increased distinctly due to the dimensions of width of crystals and pore sizes reduced. Although the width of crystals is reduced significantly to nanoscale, the fibrious OCP nanocrystals are bundling in parallel to form the crystal bunches. Such a biomimic multiscale porous structure of the OCP/SF composite coating could

DOI: 10.1021/am5088488
ACS Appl. Mater. Interfaces 2015, 7, 5634–5642

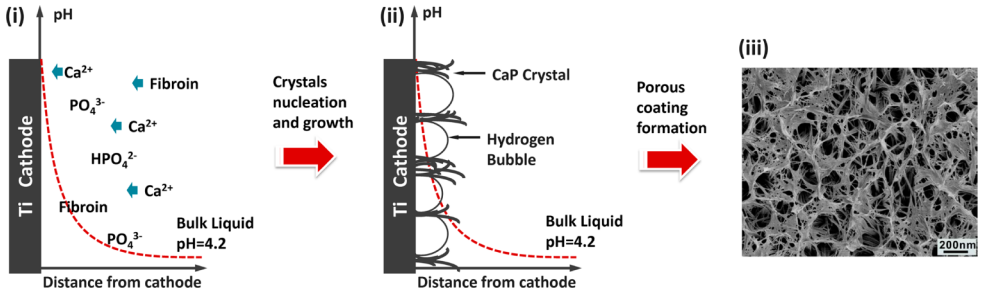

Figure 12. Schematic illustration of sequential stages in the formation of OCP/SF composite coatings on Ti substrate by ED technique. (i) Initiation of the process of ED; (ii) The bubble formation on the Ti substrate; (iii) Final porous coating of SF/OCP fibrils.

provide a sufficient space for cell anchoring, spreading, and a well-fed micro environment for the cell growth into the materials due to its run-through structure. These findings clearly demonstrate an important asset of OCP/SF composite coatings with a nano-micro multiscale porous structure presented in this study.

Reconstruction of damaged load-bearing hard tissue is one of the major concerns in tissue engineering. Challenges include selecting the optimal biomaterial and the design of an appropriate framework for cell growth and tissue development. Our goal in this study was to design and fabricate a vital composite material for hard tissue engineering and to test the prepared samples for cell seeding suitability and effectiveness in promoting cells growth.

In the present work, a unique highly ordered OCP/SF composite coating with nano-micro multiscale structure on Ti substrate was constructed successfully by ED technique. In vitro cell culture results clearly show that the OCP/SF composite coating was easily and effectively seeded by the simple method of pipetting a cell suspension evenly onto it. In comparison with the OCP coating, the nano-micro multiscale structure and the larger surface area volume ratio of the OCP/SF coating facilitates cell attachment and provides sufficient area for cell growth.

Based on experimental results and electrochemical deposition mechanisms of calcium phosphate coatings on metals,[38−40] the proposed construction mechanism of the OCP/SF coating is illuminated in Figure 12. When a current passes through the electrodes, OH^- ions are initially generated at the cathode surface due to the electrochemical reactions of water. As a result, the pH value at the interface of cathode/solution is higher than that in bulk electrolyte. The higher pH increases the supersaturation of CaP and leads to the precipitation of the various CaP phases on the surface of Ti cathode: $Ca_{10}(PO_4)_6(OH)_2$ (HAp), $Ca_2(PO_4)_3{\cdot}nH_2O$ (TCP), $CaHPO_4{\cdot}2H_2O$ (DCPD), and OCP.[41] The ED parameters, such as current density, temperature, electrolyte concentration, and deposition time are all controlled precisely in order to set up an appropriate deposition environment to facilitate the OCP precipitation and thereby possibly enhancing the phase selective effect of the Ca−P system. It was noted that the phase simplicity increases structure controllability. It is interesting to recall that the structures of the prepared OCP/SF coatings and OCP coating are distinctly different as in Figure 1. SF plays an important role in constructing the unique nano-micro two-level biomimetic structure of OCP/SF composite coating. The isoelectric point of SF is approximately at pH 4.5.[42] When adding SF into the electrolyte, SF is positively charged. Under effect of electric field, SF molecules (positive change) in electrolyte are driven to the vicinity of the cathode. Until SF molecules near the cathode, the higher pH value (larger than isoelectric point of SF) in the vicinity of the cathode lead to SF bring the negatively charge. Such negatively charged SF molecules can interact strongly with oppositely charged Ca^{2+} ions; however, inherent basic amino groups of SF simultaneously interact weakly with phosphate anions. Finally, the SF and OCP mineral can be coprecipitated onto the cathode by the charge and molecular interaction between protein and mineral. Additionally, once nucleation of OCP has occurred, free SF molecules adsorb on the growing OCP crystals to inhibit the growth kinetics of OCP in the specific crystalline face. Therefore, the dimensions of OCP crystals are greatly reduced to the nano scale in the presence of SF (Figure 1e). Then, accompanying growth of the OCP nano fibrils, the microlevel porous structure is constructed following the template of hydrogen bubble generation at the interface of the cathode/electrolyte during the ED process (Figure 1d,e).[43]

5. CONCLUSIONS

In summary, an OCP/SF composite coating with nano-micro multiscale porous structure on titanium substrate was successfully fabricated via ED method. Our results indicate that SF can inhibit the growth of OCP crystals and lead to the formation of nanosized OCP crystalline fibrils. Combined with the role of the hydrogen bubble template on the metal surface during the ED process, a hierarchical structure of composite coatings crossing the multiscales is formed. Furthermore, it was found that the OCP/SF composite coating plays a significant role in promoting cell adhesion, spreading, and proliferation, arising from its unique multiscale structure and appropriate chemical composition.

Our results have demonstrated the relatively simple methodology and the superior performance of the multiscale porous OCP/SF composite coatings. Such bioinspired materials possess extensive potential for application in hard tissue engineering to repair osteogenetic defects, especially in some load-bearing osteoregenerative, and also suitable as a dental implant biomaterial.

AUTHOR INFORMATION

Corresponding Authors

* E-mail: whui@suda.edu.cn. Tel: +86-512-67061169.
* E-mail: kqzhang@suda.edu.cn. Tel: +86-512-67061169.

Notes

The authors declare no competing financial interest.

DOI: 10.1021/am5088488
ACS Appl. Mater. Interfaces 2015, 7, 5634−5642

■ ACKNOWLEDGMENTS

The authors are grateful for the support from the National Science Foundation of China under Grants 51203108, 51073113, 91027039, and 51373110, the Natural Science Foundation of Jiangsu Province of China under Grants BK2011355 and BK20130313, Natural Science Foundation of the Jiangsu Higher Education Institutions of China under Grants 11KJB430011 and 10KJA540046, and the Nanotechnology Foundation of Suzhou under Grant ZXG2013037. We also acknowledge support from the Priority Academic Program Development of Jiangsu Higher Education Institutions (PAPD), Qing Lan Project for Excellent Scientific and Technological Innovation Team of Jiangsu Province (2012), and Project for Jiangsu Scientific and Technological Innovation Team (2013).

■ REFERENCES

(1) Liu, K. S.; Jiang, L. Bio-inspired Design of Multiscale Structures for Function Integration. *Nano Today* **2011**, *6*, 155−175.
(2) Liu, K. S.; Jiang, L. Multifunctional Integration: From Biological to Bio-Inspired Materials. *ACS Nano* **2011**, *5*, 6786−6790.
(3) Koch, K.; Bhushan, B.; Barthlott, W. Prog. Multifunctional Surface Structures of Slants: An Inspiration for Biomimetics. *Mater. Sci.* **2009**, *54*, 137−178.
(4) Bhushan, B.; Jung, Y. C. Natural and Biomimetic Artificial Surfaces for Superhydrophobicity, Self-cleaning, Low Adhesion, and Drag Reduction. *Prog. Mater. Sci.* **2011**, *56*, 1−108.
(5) Lakes, R. Materials with Structural Hierarchy. *Nature* **1993**, *361*, 511−515.
(6) Fratzl, P.; Gupta, H. S.; Paschalis, E. P.; Roschger, P. Structure and Mechanical Quality of the Collagen−mineral Nano-composite in Bone. *J. Mater. Chem.* **2004**, *14*, 2115−2123.
(7) Wang, H.; Lin, C. J.; Hu, R.; Zhang, F.; Lin, L. W. A Novel Nano-micro Structured Octacalcium Phosphate/ Protein Composite Coating on Titanium by Using an Electrochemically Induced Deposition. *J. Biomed. Mater. Res., Part A* **2008**, *87*, 698−705.
(8) Wang, R. C. C.; Hsieh, M. C.; Yang, S. P.; Chuang, P. K.; Lin, J. C.; Yang, C. Y.; Lee, T. M. Characteristics and Cyto-compatibility of Collagen/Ca−P Coatings on Ti6Al4V Substrate. *Surf. Coat. Technol.* **2011**, *205*, 4683−4689.
(9) de Jonge, L. T.; Leeuwenburgh, S. C.; van den Beucken, J. J.; te Riet, J.; Daamen, W. F.; Wolke, J. G.; Scharnweber, D.; Jansen, J. A. The Osteogenic Effect of Electrosprayed Nanoscale Collagen/calcium phosphate Coatings on Titanium. *Biomaterials* **2010**, *31*, 2461−2469.
(10) Song, J. Y.; Kim, S. G.; Lee, J. W.; Chae, W. S.; Kweon, H. Y.; Jo, Y. Y.; Lee, J. J.; Lee, Y. C.; Choi, J. Y.; Kim. Accelerated Healing with the Use of a Silk Fibroin Membrane for the Guided Bone Regeneration Technique. *Oral. Surg. Oral. Med. Oral. Pathol. Oral. Radiol. Endod.* **2011**, *112*, e26−e33.
(11) Correia, C.; Bhumiratana, B.; Yan, L. P.; Oliveira, A. L.; Gimble, J. M.; Rockwood, D.; Kaplan, D. L.; Sousa, R. A.; Reis, R. L.; Novakovic, G. V. Development of Silk-based Scaffolds for Tissue Engineering of Bone from Human Adipose-derived Stem Cells. *Acta Biomater.* **2012**, *8*, 2483−2492.
(12) Park, S. J.; Lee, K. Y.; Ha, W. S.; Park, S. Y. Structural Changes and Their Effect on Mechanical Properties of Silk Fibroin/Chitosan Blends. *J. Appl. Polym. Sci.* **1999**, *74*, 2571−2575.
(13) Kweon, H.; Ha, H. C.; Um, I. C.; Park, Y. H. Physical Properties of Silk Fibroin/Chitosan. *J. Appl. Polym. Sci.* **2001**, *80*, 928−934.
(14) Minoura, N.; Aiba, S.; Gotoh, Y.; Tsukada, M.; Imai, Y. Attachment and Growth of Cultured Fibroblast Cells on Silk Protein Matrices. *J. Biomed. Mater. Res.* **1995**, *29*, 1215−1221.
(15) Arai, T.; Freddi, G.; Innocenti, R.; Tsukada, M. Biodegradation of *Bombyx mori* Silk Fibroin Fibers and Films. *J. Appl. Polym. Sci.* **2004**, *91*, 2383−2390.
(16) Liang, M. N.; Yao, J. R.; Chen, X.; Huang, L.; Shao, Z. Z. Silk Fibroin Immobilization on Poly(ethylene terephthalate) Films: Comparison of Two Surface Modification Methods and Their Effect on Mesenchymal. *Mater. Sci. Eng., C* **2013**, *33*, 1409−1416.
(17) Vepari, C.; Kaplan, D. L. Silk as a Biomaterial. *Prog. Polym. Sci.* **2007**, *32*, 991−1007.
(18) Ko, J. S.; Yoon, K.; Ki, C. S.; Kim, H. J.; Bae, D. G.; Lee, K. H.; Park, Y. H.; Um, I. C. Effect of Degumming Condition on the Solution Properties and Electrospinnablity of Regenerated Silk Solution. *Int. J. Biol. Macromo.* **2013**, *55*, 161−168.
(19) Ho, M. P.; Wang, H.; Lau, K. T. Effect of Degumming Time on Silkworm Silk Fibre for Biodegradable Polymer Composites. *Appl. Surf. Sci.* **2012**, *258*, 3948−3955.
(20) Wang, H.; Liu, X. Y.; Chuah, Y. J.; Goh, J. C. H.; Li, J. L.; Xu, H. Y. Design and Engineering of Silk Fibroin Scaffolds with Biomimetic Hierarchical Structures. *Chem. Commun.* **2013**, *49*, 1431−1433.
(21) Meine, L.; Hofmann, S.; Karageorgiou, V.; Head, C. K.; Cool, J. M.; Gronowicz, G.; Zichner, L.; Langer, R.; Novakovic, G. V.; Kaplan, D. L. The Inflammatory Responses to Silk Films *In Vitro* and *In Vivo*. *Biomaterials* **2005**, *26*, 147−155.
(22) Altman, G. H.; Horan, R. L.; Lua, H. H.; Moreau, J.; Martin, I.; Richmond, J. C.; Kaplan, D. L. Silk Matrix for Tissue Engineered Anterior Cruciate Ligaments. *Biomaterials* **2003**, *23*, 4131−4141.
(23) Santin, M.; Motta, A.; Freddi, G.; Cannas, M. *In Vitro* Evaluation of the Inflammatory Potential of the Silk Fibroin. *J. Biomed. Mater. Res.* **1999**, *46*, 382−389.
(24) Brown, W. E.; Smith, J. P.; Lehr, J. R.; Frazier, A. W. Crystallographic and Chemical Relation between Octacalcium Phosphate and Hydroxyapatite. *Nature* **1962**, *196*, 1050−1055.
(25) Iijima, M.; Kamemizu, H.; Wakamatsu, N.; Goto, T.; Doi, Y.; Moriwaki, Y. Transition of Octacalcium Phosphate to Hydroxyapatite in Solution at pH 7.4 and 37 °C. *J. Cryst. Growth* **1997**, *181*, 70−78.
(26) Kamakura, S.; Sasano, Y.; Shimizu, T.; Hatori, K.; Suzuki, O.; Kagayama, M.; Motegi, K. Implanted Octacalcium Phosphate is More Resorbable than β-tricalcium Phosphate and Hydroxyapatite. *J. Biomed. Mater. Res.* **2002**, *59*, 29−34.
(27) Habibovic, P.; Vandervalk, C. M.; Vanblitterswijk, C. M.; Degroot, K. Influence of Octacalcium Phosphate Coating on Osteoinductive Properties of Biomaterials. *J. Mater. Sci. Mater. Med.* **2004**, *15*, 373−380.
(28) Webster, T. J.; Siegel, R. W.; Bizios, R. Osteoblast Adhesion on Nanophase Ceramics. *Biomaterials* **1999**, *20*, 1221−1227.
(29) Murugan, R.; Ramakrishna, S. Development of Nanocomposites for Bone Grafting. *Compos. Sci. Technol.* **2005**, *65*, 2385−2406.
(30) Webster, T. J.; Ergun, C.; Doremus, R. H.; Siegel, R. W.; Bizios, R. Enhanced Functions of Osteoblasts on Nanophase Ceramics. *Biomaterials* **2000**, *21*, 1803−1810.
(31) Liu, H. N.; Webster, T. J. Nanomedicine for Implants: A Review of Studies and Necessary Experimental Tools. *Biomaterials* **2007**, *28*, 354−369.
(32) Zhang, Q. Y.; Leng, Y.; Xin, R. L. A comparative Study of Electrochemical Deposition and Biomimetic Deposition of Calcium Phosphate on Porous Titanium. *Biomaterials* **2005**, *26*, 2857−2865.
(33) Lu, X.; Zhao, Z. F.; Leng, Y. Calcium Phosphate Crystal Growth under Controlled Atmosphere in Electrochemical Deposition. *J. Cryst. Growth* **2005**, *284*, 506−516.
(34) Wang, J. M.; Apeldoorn, A. V.; Groot, K. D. Electrolytic Deposition of Calcium Phosphate/Chitosan Coating on Titanium Alloy: Growth Kinetics and Influence of Current Density, Acetic Acid, and Chitosan. *J. Biomed. Mater. Res., Part A* **2006**, *76*, 503−511.
(35) Zhang, Y. Z.; Ouyang, H. W.; Lim, C. T.; Ramakrishna, S.; Huang, Z. M. Electrospinning of Gelatin Fibers and Gelatin/PCL Composite Fibrous Scaffolds. *J. Biomed. Mater. Res. Part B: Appl. Biomater.* **2005**, *72B*, 156−65.
(36) Tamada, Y. New Process to Form a Silk Fibroin Porous 3-D Structure. *Biomacromolecules* **2005**, *6*, 3100−3106.
(37) Borsari, V.; Giavaresi, G.; Fini, M.; Torricelli, P.; Salito, A.; Chiesa, R.; Chiusoli, L.; Volpert, A.; Rimondini, L.; Giardino, R. Physical Characterization of Different-Roughness Titanium Surfaces, With and Without Hydroxyapatite Coating, and Their Effect on

DOI: 10.1021/am5088488
ACS Appl. Mater. Interfaces 2015, 7, 5634−5642

Human Osteoblast-Like Cells. *J. Biomed. Mater. Res. B Appl. Biomater.* **2005**, *75*, 359−368.
(38) Zhang, J. M.; Lin, C. J.; Feng, Z. D.; Tian, Z. W. Mechanistic Studies of Electrodeposition for Bioceramic Coatings of Calcium Phosphates by an *In Situ* pH-Microsensor Technique. *J. Electroanal. Chem.* **1998**, *452*, 235−240.
(39) Kar, A.; Raja, K. S.; Misra, M. Electrodeposition of hydroxyapatite onto Nanotubular TiO_2 for Implant Applications. *Surface Coat. Technol.* **2006**, *201*, 3723−3731.
(40) Kuo, M. C.; Yen, S. K. The Process of Electrochemical Deposited Hydroxyapatite Coatings on Biomedical Titanium at Room Temperature. *Mater. Sci. Eng. C* **2002**, *20*, 153−160.
(41) Koutsoukos, P.; Amjad, Z.; Tomson, M. B.; Nancollas, G. H. Crystallization of Calcium Phosphates. A Constant Composition Study. *J. Am. Chem. Soc.* **1980**, *102*, 1553−1557.
(42) Chen, J.; Minoura, N. Transport of Pharmaceuticals through Silk Fibroin Membrane. *Polymer* **1993**, *35*, 2853−2856.
(43) Li, Y.; Song, Y. Y.; Yang, C. Hydrogen Bubble Dynamic Template Synthesis of Porous Gold for Nonenzymatic Electrochemical Detection of Glucose. *Electrochem. Commun.* **2007**, *9*, 981−988.

DOI: 10.1021/am5088488
ACS Appl. Mater. Interfaces 2015, 7, 5634−5642